J. MORVILLE[*]
D. ROMANINI[✉]
A.A. KACHANOV[**]
M. CHENEVIER

Two schemes for trace detection using cavity ringdown spectroscopy

Laboratoire de Spectrométrie Physique – CNRS UMR 5588, Université J. Fourier– Grenoble I, B.P. 87 – 38402 Saint Martin d'Hères Cedex, France

ABSTRACT We describe and compare two schemes of high-sensitivity cavity ringdown spectroscopy (CRDS), both functioning with telecom diode lasers. The first (cw-CRDS) gives high spectral resolution, which is useful for low-pressure trace detection or for laboratory spectroscopy applications. We present a compact prototype partly based on fiber technology. The second scheme exploits optical feedback (of-CRDS) and results in a much simpler setup, more appropriate for realizing low-cost trace-detection devices.

PACS 42.62.Fi; 87.64.Ni; 42.68.Ca; 82.80.Gk

1   Introduction

There is today a growing need for compact and fast trace-gas detectors for application to environmental monitoring, medical diagnostics, gas handling, semiconductor and chemical process control, etc. Laser absorption spectroscopy can provide accurate and quantitative in-situ concentration measurements with fast response and recovery time, large dynamic range, and high discrimination among different coexisting species. When coupled with monolithic semiconductor lasers, absorption spectroscopy appears to be most appropriate for detecting small molecules presenting isolated absorption lines. For example, DFB (distributed feedback) laser diodes, which are widely used in telecommunication applications, are compact and robust and possess a small but continuous wavelength-tuning range which easily spans a few molecular absorption lines. More recently admitted into the telecom arena, VCSELs (vertical-cavity surface-emitting lasers) are also of high interest for absorption spectroscopy, but the wavelength range where commercial devices are available is still rather limited.

Small molecules such as CO_2, CO, CH_4, H_2S, C_2H_2, H_2O, HF, and HCl all present narrow and strong fundamental vibrational transitions beyond $2\,\mu m$. Overtone transitions falling in the 1–2-μm range are one to two orders of magnitude less intense, which can be compensated by using a high-sensitivity technique. The premium is that in this spectral region DFB diode lasers and InGaAs photodiodes developed for telecommunications are readily available at low mass-production costs. These devices have higher performance, at room temperature, compared to their longer-wavelength analogues, lead-salt diodes and quantum-cascade lasers, which mostly operate at cryogenic temperatures. The narrow tuning range of all these semiconductor lasers implies that one source at a given wavelength may be used for optimal detection of a single species. However, multi-source devices [1] become convenient using compact room-temperature diode lasers of high electric efficiency.

Cavity ringdown spectroscopy (CRDS) is a versatile high-sensitivity absorption technique [2–22] which, since its introduction and for about ten years, has been exclusively used with pulsed nanosecond lasers. It is the only simple way to obtain quantitative absorption spectra of high sensitivity with such noisy sources. Published results demonstrate a detection limit (noise-equivalent absorption) ranging from 10^{-6} /cm (in the UV range) to 10^{-10} /cm, comparable to what can be achieved by photoacoustic spectroscopy or by intracavity laser absorption [23, 24]. A fundamental fact for trace detection, it has been shown that CRDS yields reliable absolute absorption measurements [4, 8, 9, 18], as expected when considering its working principle. In fact, CRDS directly measures the absolute value of optical losses in a high-finesse cavity. The intracavity sample absorption per pass is obtained as a variation of cavity losses when the sample is admitted into the cavity, or when the wavelength is tuned around an absorption line. Finally, CRDS is insensitive to source-intensity noise, which is an important advantage over most spectroscopic techniques.

In 1997 we introduced a first CRDS scheme working with narrow-band cw lasers (cw-CRDS) [14–16]. Here, the challenge lies in the efficient coupling of narrow-band laser radiation into even narrower cavity resonances. Our scheme appears to be the general solution to this problem, offering the best compromise of simplicity and performance when compared to other solutions [25–28]. This is proven by the number of spectroscopic results our scheme has already produced and the extreme detection limits it has allowed, reaching down to 10^{-11} cm^{-1} Hz$^{-1/2}$ [22, 24, 29–34].

✉ Fax: +33-476/635-495, E-mail: daniel.romanini@ujf-grenoble.fr
[*]*Current address:* LASIM, 43 Bvd. 11 Novembre 1918, 69 622 Villeurbanne, France
[**]*Current address:* Picarro, Inc., 480 Oakmead Parkway, Sunnyvale, CA 94085, USA

Besides permitting unprecedented measurements in high-resolution spectroscopy [34], cw-CRDS opened the way to compact diode-laser CRDS trace-detection devices. However, the need for an even more compact and rugged setup using fewer (and less expensive) optical components led us to develop a second scheme. This is based on optical feedback (of-CRDS) for improving cavity injection by a DFB diode laser [35–37]. Given this restriction with respect to the laser source, of-CRDS is evidently a less general approach than cw-CRDS.

In the following, we will present and compare these two CRDS schemes when applied to DFB diode lasers. As CRDS is now a widely accepted technique with more than a hundred applications published per year [38–40], the interested reader will find all the necessary background in the cited literature.

2   CRDS with cw lasers: a fibered cw-CRDS setup

To our knowledge, some of the earliest light-decay measurements in optical cavities were exploited by Anderson and co-workers in 1984 to determine the reflectivity of dielectric mirrors [41]. When coupling a cw narrow-band laser (e.g. a HeNe laser) to an optical cavity, occasional resonance of the laser frequency with a cavity mode was observed as giving bursts of spikes of transmitted light. Such occasional coincidences are due to slow (thermal or acoustic) fluctuations of laser frequency and cavity length. An optical switch was triggered to interrupt the laser beam during a transmission spike, thus allowing a clean exponential decay of the light injected into the cavity. From the time constant of the exponential decay, cavity losses were directly and accurately determined. Unfortunately, at the time no measurement of intracavity absorption by a gas was tried, and this technique had to wait until recently for an application to absorption spectroscopy. The main problem to be solved was that occasional cavity injection is too inefficient for obtaining extensive absorption spectra.

It is surprising that for a period of more than ten years the simple idea of cw-CRDS remained unexploited. Meanwhile, CRDS became known as a high-sensitivity absorption technique for use with pulsed lasers. Injecting a cavity with high peak power pulses is intuitively appealing, as frequency matching is not needed since the pulse spectrum is usually larger than the cavity mode spacing. Given the high laser peak power, the small fraction of a pulse transmitted by the cavity input mirror is enough to produce an easily detectable signal at the cavity output. The laser pulse is thus attenuated and diluted in time, reducing the danger of unwanted nonlinear effects usually associated with high peak powers.

When coming to cw lasers, their narrow emission spectrum and low power level seem to imply that frequency locking is necessary for acceptable cavity injection. It is well known that a large intracavity buildup of the photon field occurs when the frequency of a cw laser coincides with one of the cavity resonances, but locking a laser to a resonance only a few tens of kHz wide is a daunting task. We believe that for several years considerations of this sort must have been a strong inhibition to try and use cw lasers for CRDS. Our cw-CRDS scheme is a simple improvement to Anderson's reflectometer, where we have introduced a cavity-length

modulation. This removes the occasional character of injection events and gives a steady periodic occurrence of passages through resonance, with repetition rates up to several hundred Hertz.

CW-CRDS setups for spectroscopy with dye lasers or external cavity diode lasers (ECDLs) have already been described and explained in much detail [14, 15]. With respect to the fibered DFB-laser setups presented here, for which there are a couple of similar systems recently described [1, 42], we will then focus only upon specific issues not previously addressed.

Fibered optical components are readily available on the telecom market for the spectral range 1.3 to 1.6 μm. Custom components anywhere else in the 1–2-μm range may also be custom made, at consequently higher prices. Most fibered components come with single-transverse-mode input and output low-loss plug&play optical connectors. For our cw-CRDS device, whose setup is shown in Fig. 1, we used fibered components wherever possible (with low-feedback FC/APC connectors). As an immediate benefit, the fibered part of our system should satisfy rather tight industrial specifications.

In order to avoid perturbation of the laser source, good optical isolation is needed. Butterfly-packaged telecom DFB lasers including a 30-dB optical isolator are today available for a few hundred euros at any specified wavelength in the range 1480–1630 nm. They produce tens of mW for several years of continuous operation, and the packaging includes a Peltier and a thermistor for laser-temperature stabilization, a power-monitoring photodiode, and sometimes even a thin etalon for an absolute wavelength reference.

In our setup, an additional fibered optical isolator is connected to the laser, followed by a fibered acousto-optic switch (AOS). These are installed inside a closed chassis ($30 \times 30 \times 15 \, \text{cm}^3$) together with control electronics, a fibered photodiode, and an industry-standard Pentium motherboard. This includes a PC card (ADLINK PCI9118) carrying one 12-bit, 300-kHz digitizer (A/D) for sampling the ringdown signal and two 12-bit D/A outputs for controlling temperature and
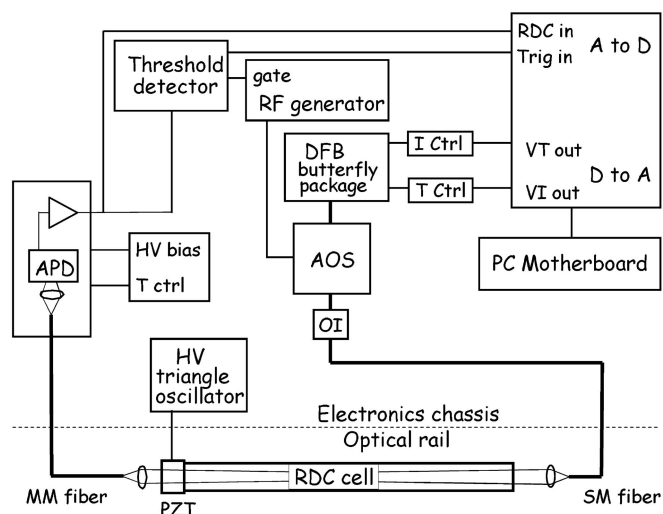

FIGURE 1   CW-CRDS setup: DFB is a fibered telecom laser, OI is an optical isolator, AOS is an acousto-optic switch, APD is a fibered avalanche photodiode, SM and MM are single- and multi-mode fibers, PZT is a piezoelectric actuator, and A and D stand for analog and digital, respectively

current of the DFB laser. Given the relatively low cavity injection signal in cw-CRDS, a sensitive InGaAs avalanche photodiode (APD) is used (Epitaxx model ETX240). This ensemble weighs about 3 kg and requires a ± 15 V/1 A and 5 V/8 A external power supply.

With regard to the AOS, this type of optical switch is the best choice to date given its large on/off contrast ($> 10^5$), fast beam shut-off (100 ns), and reasonably short response delay ($\sim 2\,\mu$s). This delay however allows important changes of cavity injection to occur between the time when the cavity transmission goes above the threshold and the time when the injection is interrupted. This was barely a noticeable effect in previous cw-CRDS setups involving lasers spectrally narrower (FWHM < 100 kHz on the time scales of cavity buildup) [14, 15] than DFB diodes (FWHM > 1 MHz). A larger line width corresponds to faster field phase fluctuations, which translate into faster amplitude fluctuations at cavity output [43]. As a result, the sampled decay signal does not start at the pre-set threshold level: fluctuations of more than 50% in excess or defect are observed. This should have a noise penalty due to nonlinearities in the response of amplification and digitization circuits. When we observe the shot-to-shot fluctuations of the ringdown time at fixed laser frequency we find that they are about three times larger than the standard deviation of the exponential fit of a single event, which confirms the presence of excess noise.

All open-path optics are placed on a linear rail about 1-m long, with a single-mode fiber delivering laser radiation to one end of the vacuum-tight ringdown cell, which is 60-cm long (free spectral range (FSR) $\simeq 250$ MHz). A single lens images the diverging fiber output into the TEM$_{00}$ cavity mode, according to Gaussian optics calculations. In fact, the single-mode fiber plays here the same spatial-filtering role as the pinhole in previous cw-CRDS setups [14, 15].

The cavity mirrors are mounted on tilt stages, one including a piezoelectric tube for modulating the cavity length by slightly more than $\sim \lambda/2$, which makes the cavity modes oscillate by more than one FSR. The maximum modulation rate permitted by our high-voltage oscillator is about 400 Hz, which gives a maximum ringdown repetition rate of 800 Hz. The effective data rate is somewhat lower. First of all, a fraction of passages through resonance may not go above threshold. Secondly, each ringdown is independently sampled and analyzed using a linear fit after taking the logarithm of the signal. Thus, when two events fall too close in time only one event can be processed. This notably happens when the passage through resonance is close to the cavity modulation turning point.

It is interesting to note that if we increase the cavity modulation rate further we should start losing injection efficiency since [43], given the large DFB laser line width (typically 2–3 MHz), the duration of a passage through resonance is already comparable to the cavity response time (3 MHz/(800 Hz $\times$ 250 MHz) $\simeq 10\,\mu$s). On the other hand, we verified that when we change the cavity modulation rate to 400 Hz, there is no important change in the average injected intensity during passages through resonance. We also remark that no cavity 'tracking' is used here. This was introduced for increasing performance in previous setups with ECDLs [15], which have a much narrower line width (<100 kHz on ms

time scales). Tracking allows the reduction of the cavity modulation amplitude, thus increasing the frequency of passages through resonance while keeping constant the duration of passages through resonance. Here tracking could also be used for improving the data-acquisition rate, but it would make the system sensitive to vibrations. Instead, as the cavity length is modulated by one full FSR, external vibrations are of no consequence.

The cavity output is injected by a short focal length lens into a 60-μm-core (multi-mode) fiber, which conveys the signal back to the APD. While it would be simpler to place the APD near to the cavity output, wide variations of external temperature would make its thermal stabilization difficult. Indeed, for high-gain operation ($\sim \times 40$) we set the APD bias very close to its breakdown voltage (~ 53 V at 20 °C), which is strongly temperature dependent. The setup was originally conceived as a prototype which could fly on a stratospheric balloon: placing the electronics, the laser, and the APD inside a closed chassis would make it easy to maintain them close to room temperature. On the other hand, the mechanics composing the optical rail should be engineered to be stable down to temperatures as low as −60 °C.

The APD signal is boosted by a 500-kΩ transimpedance amplifier with a band pass close to the sampling rate of the D/A card. A program running under DOS insures laser-diode tuning by current or temperature steps, and real-time calculation of the ringdown rate from the digitized signal at a repetition rate compatible with the cavity modulation (up to 800 Hz).

Finally, besides the cavity mirrors' tilt, the only other fine optical adjustments needed are provided by translation stages for the two lenses. It is also important that lenses and fiber input facets be slightly tilted with respect to the optical axis to avoid etaloning effects on the CRDS spectra [4]. The mirrors should also be slightly wedged for the same reason.

3   OF-CRDS: experimental setup and principle of operation

The second CRDS scheme we developed for DFB diode lasers is appealing for applications where budget is a critical factor and a compromise on performance is acceptable. Coupling of diode lasers to cavities by optical feedback has been for a long time a known means in atomic physics either for spectral narrowing and stabilization of diode lasers [44] or for building-up high intracavity fields [45]. Optical feedback from the cavity to the diode laser may therefore be exploited rather than avoided, which also makes optical isolators unnecessary. Since optical feedback makes cavity injection efficient, a high-gain avalanche photodiode is no longer needed. Finally, we will see that the fast on/off capabilities of diode lasers may be also exploited to eliminate the AOS from our setup. All this is balanced by an increased complexity of the physics underlying of-CRDS compared to cw-CRDS.

The simple V-shaped cavity of Fig. 2 allows optical feedback only from inside the cavity (at resonance), since the direct reflection from the input mirror does not come back to the source. The feedback rate (fraction of laser power returning as feedback) is adjusted using a variable attenuator. Given the large per-pass amplification of diode lasers, their short cavity
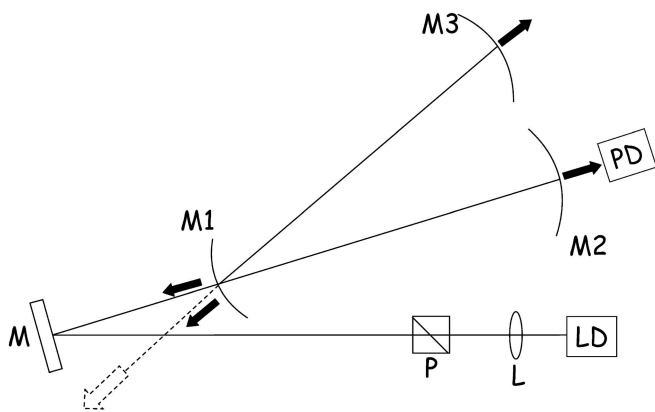
FIGURE 2 OF-CRDS scheme: LD is the DFB laser diode collimated by lens L, P is a polarizer used as a variable attenuator, M is a steering mirror, M1, M2, M3 are the high-reflectivity concave mirrors of the V-shaped ringdown cavity, and PD is a PIN photodiode

length, and its low to a finesse, returning light has a strong effect. Frequency locking V-cavity resonance is observed with a feedback rate as small as 10^{-6}, and is accompanied (and enhanced) by the narrowing of the laser spectrum [46]. Spectral narrowing is a direct consequence of the filtering ability of the cavity, which returns only a narrow selection of the laser spectrum. If the returning field has the right phase (which depends on laser–cavity distance) the laser amplifies this 'seeding' signal and its spectrum becomes narrower, which improves still further cavity injection. Eventually, the laser spectrum becomes even narrower than the cavity mode and the self-reinforcing optical locking loop reaches a steady state within the cavity response time (tens of microseconds in our case). The laser remains locked to the resonance as long as its driving current remains inside some interval ('locking range'), whose width increases with the feedback rate. Finally, if locking lasts long enough compared with the cavity response time (depending on laser tuning speed and locking range), buildup of the intracavity field becomes complete, as if the cavity was injected by a monochromatic field.

Fundamental results in laser-diode optical self-locking, both experimental and theoretical, may be found in a few excellent publications [46–48]. These deal with the case when the laser frequency is stationary ('adiabatic' regime), but in practice the same treatment applies if laser tuning is sufficiently slow. The basics of self-locking necessary for understanding of-CRDS concern the role of three parameters: Feedback phase and rate, and laser tuning speed.

First, let us consider the feedback phase. In the adiabatic regime, the feedback field from buildup inside the cavity goes through a complete phase reversal ($-\pi/2$ to $\pi/2$) as the laser frequency goes through a resonance. At the same time, the intracavity buildup goes through a maximum (for zero phase). The actual feedback phase at the laser will be additionally shifted by $\Delta\varphi = 2\pi D/\lambda$, where D is the cavity–laser distance. According to semiconductor laser dynamics there is a value of the phase φ_0 for which the feedback field at the laser will have maximum effect in terms of line-width narrowing and frequency locking. During a passage through resonance the locking will then be maximum if the cavity phase at resonance (zero) plus $\Delta\varphi$ matches φ_0 (modulo 2π). However, since the phase reversal occurs almost completely inside the cavity res-

onance width, the feedback field will still go through φ_0 for a large interval of $\Delta\varphi$ values. This introduces a large tolerance in the laser–cavity distance; thus feedback locking will almost always occur even if with reduced intensity (given the slight off-resonance phase-crossing point).

With respect to the feedback rate (at a fixed laser–cavity separation), its effect is rather simple. The locking range will increase with the feedback rate. As long as the passage through resonance occurs in the adiabatic regime, the locking range is independent of the tuning speed.

However, when the laser tuning speed becomes too large, the duration of a passage through resonance does not allow sufficient intracavity buildup, and the feedback level remains too low for frequency locking. The cavity injection rapidly drops down to the levels one can observe without feedback. We are then outside the stationary (or adiabatic) regime where the optical locking theory may be applied. In practice, we observe the injection of cavity modes becoming unstable beyond a certain tuning speed, which increases with the feedback rate [49].

It should now be rather clear how ringdowns may be produced and observed when feeding the laser with periodic rectangular pulses (several hundreds of µs) of a given current level. At the beginning of each pulse the laser makes a fast frequency sweep which progressively slows down when approaching the equilibrium frequency corresponding to the given current level (see Fig. 3). By increasing the pulse duration, the frequency-tuning speed at the end of the pulse becomes slower. This allows adjusting the tuning speed until good optical locking is observed, on average, at the end of the pulses. The feedback rate is also adjusted by the variable attenuator to obtain a locking range comparable to the cavity mode spacing (more details below). Ringdowns are then often observed with sufficient intensity to be digitized and fitted at the falling edge of the pulses, where the laser emission abruptly stops. For frequency tuning, it is simple enough to change the pulse current level. A convenient feature is that, while the laser frequency at the end of the pulses follows this change, the tuning speed (at the end of the pulses) is practically unaffected. Slower but broader tuning may also be achieved by changing the laser temperature (~ 0.1 nm/°C typically) at fixed pulse intensity.

Rather than trying to control the phase, which requires sub-lambda stabilization of the laser–cavity distance, we modulate this distance by introducing mechanical vibrations, for example by placing the small pump, which circulates ambient air into the ringdown cavity, directly on the optical rail. For the feedback rate and tuning speed we use, there is a high chance of sampling a ringdown signal of large intensity at the end of a pulse (70 to 80%), with signal intensities (at the beginning of the ringdown) in the 1–10-µW range. This is typical for a laser intensity of a few milliwatts and takes into account the laser attenuation needed for a suitable feedback rate. For mirror transmissions of about 10^{-5}, the corresponding intracavity power may then rise to a few watts. At atmospheric pressure, and considering the relatively low strength of the overtone transitions used for trace detection in the 1–2-µm range, chances of saturating the molecular absorption are negligible. On the other hand, saturation effects should be considered at low pressure.
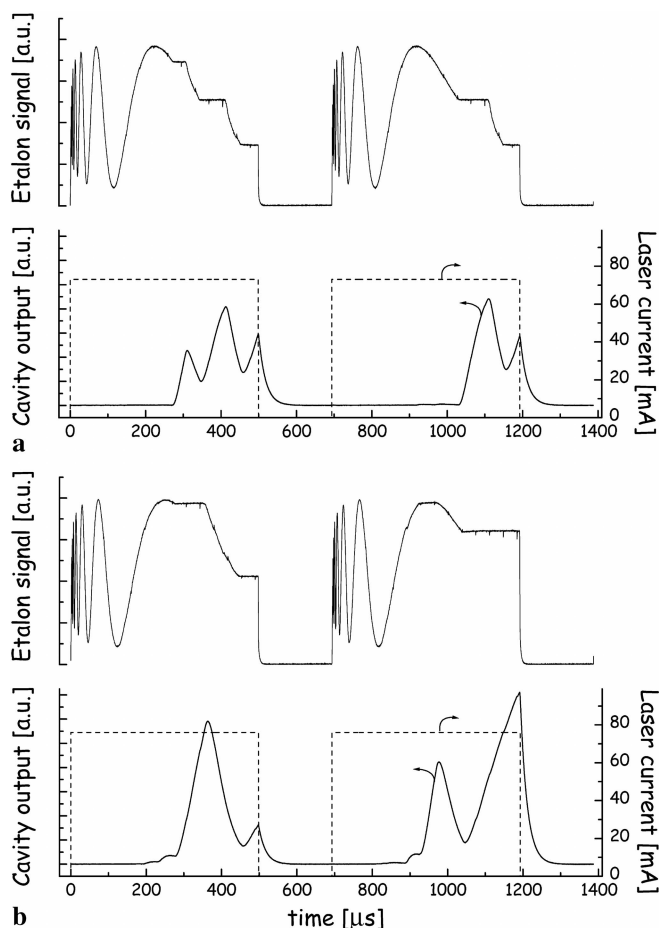
FIGURE 3 Examples of cavity injection for two feedback rates: in (**b**) the rate is about twice that in (**a**). Current pulses are applied to the diode laser (*dashed lines*). The fast laser frequency sweep which progressively slows down when approaching the end of the current pulse is demonstrated by the etalon signal (*upper traces* in (**a**) and (**b**)). Laser-frequency locking by optical feedback gives horizontal periods in the etalon traces which are simultaneous with cavity transmission peaks (*lower traces*)

The feedback rate plays a key role in our 'pulsed' injection scheme. In Fig. 3 we show signals illustrating two levels of feedback rate. The lower rate (in the range of 10^{-3}) is close to the optimal working value for our setup, while the higher rate is about twice as large. An uncoated, solid, flat Fabry–Perot (FP) etalon is added to the setup for this demonstration. A fraction of the laser radiation is directed through it by a beam splitter placed at the laser output, and the interference of reflections from the front and back etalon surfaces is monitored by a photodiode. As the laser frequency tunes, an oscillating signal is then observed, whose period is the etalon FSR (3.45 GHz here). If the laser stops tuning as it temporarily locks to a cavity mode, a flat period appears on the etalon trace. For clarity of display, only two laser pulses are plotted in the figure for each feedback rate, but they are perfectly representative of what is observed on several consecutive pulses. It is important that during these recordings mechanical vibrations were removed, leaving only slow fluctuations of the feedback phase occurring on time scales longer than several pulses.

In the higher-feedback case (Fig. 3b), a detectable signal at the cavity output starts appearing after $\sim 200\,\mu s$ from the

beginning of a pulse. Two locking periods then follow rather systematically before the pulse ends. For the lower rate, locking starts around $300\,\mu s$ but about three locking periods occur during the rest of the pulse (Fig. 3a). In fact, as the locking range is smaller, frequency jumps from one cavity mode to another are more frequent and also smaller, as can be deduced from the etalon trace. The larger locking range at higher feedback induces fewer and larger jumps between modes (which may not be next-neighbors).

Another observation is that the injection pattern from a pulse to the next is more reproducible in the low-feedback case (if the feedback phase is stable as here). The locking range being smaller than the cavity FSR, the laser locks in succession to the cavity modes without any misses. On the other hand, if the locking range is larger than the FSR, after locking to one mode the next neighboring mode is likely skipped. During a pulse, as the tuning speed decreases to levels where locking becomes possible, the first available mode has some chance not to lock since laser phase fluctuations are still relevant before locking and line narrowing take place. This lack of determinism at high tuning speeds is evident in Fig. 3a, where the first injected mode in the first laser pulse is actually missed during the second pulse, while the following modes lock reproducibly in the two pulses (they occur at lower tuning speed). At higher feedback, the first locked mode may then completely determine the ensuing history of locking modes. In Fig. 3b every other mode appears to be locking and two pulses starting with a different mode also end up with a different one.

Starting from the situation presented in Fig. 3, if we go towards higher feedback rates the locking range may be increased up to five cavity FSR's. Since optical locking is less favorable in the presence of intracavity absorption, a large locking range has the effect of making modes on the baseline close to an absorption line to lock more easily than those inside the line width. Absorption lines appear then strongly asymmetrically distorted. On the other hand, if the feedback rate is lowered, the tuning speed has to be decreased by using longer current pulses, degrading the acquisition rate. The reduced locking range goes in the same direction; as this becomes smaller than the cavity FSR the chance of observing a ringdown at the end of a pulse decreases rapidly, since the laser may go off when not locked to any cavity mode. At the end, feedback rates giving signals such as those of Fig. 3 are optimal for fast recording (at kHz rates) of undistorted absorption spectra.

We have seen that the last excited mode giving a ringdown at the end of each pulse may vary by one mode. Each spectral point is thus frequency defined with an accuracy not better than one cavity FSR. This relatively large level of frequency noise may also be considered as limiting the spectral resolution. This seems a fair price to be paid for a simpler device with a faster response for gas-concentration measurements. Nonetheless, because of the random nature of this frequency noise, averaging allows recovering absorption-line profiles of excellent quality for pressure-broadened transitions, if the locking range is not much larger than the FSR. On the other hand, a larger feedback rate and locking range (about two FSR's) may be used for trace detection. Besides allowing for shorter pulses and higher data rate, the dynamic range

is enhanced since a larger intracavity absorption is tolerated before the locking range drops below the cavity FSR.

With respect to noise in the measured ringdown time (vertical noise in the spectrum), this is dominated by a subtle effect associated with the phase of the intracavity field at the cavity folding mirror. If we consider a perfectly symmetric cavity, successive cavity modes (as usual we consider only the TEM_{00} modes) will alternatively present a node and a maximum at this mirror. This results in a different field distribution inside the multi-layer structure of the dielectric mirror, giving slightly different reflectivity and losses. In the appropriate conditions (small locking range, no vibrations, and no averaging) it is possible to clearly observe this effect as a doubling of the ringdown spectrum, with data points lying alternatively on two parallel spectra. In our of-CRDS scheme this is a true source of uncontrolled excess noise, which makes shot-to-shot variations of the ringdown time 10 to 100 times larger than the standard deviation from the fit of a single ringdown event (typically $\sigma_\tau/\tau \sim 5 \times 10^{-4}$). When vibrations are introduced, this intrinsic systematic spectral modulation can be efficiently washed out by averaging.

We end this section with technical details about the operation of our of-CRDS devices. In order to control the feedback rate we use a low-quality, low-cost polarizing plate. Since laser emission is 99% linearly polarized, rotation of the polarizer produces a variable attenuation. As the needed feedback level is less than 1%, the polarizer axis comes to be almost orthogonal to the laser polarization. If this is vertical, the beam incident onto the cavity is then almost horizontally polarized. Given the different phase shift upon reflection of P- and S-polarized light onto the folding (input) mirror of the cavity, each transverse cavity mode splits into two modes of vertical and horizontal polarizations. A sizeable difference in the reflectivity is present for the two polarizations, causing different ringdown times. When tuning the laser frequency, this goes through resonance at different times with the split polarization modes, but only those horizontally polarized have sufficient coupling to produce optical locking.

Similarly, such an accurate transverse mode matching as in cw-CRDS is not needed. As soon as the incoming beam has better overlap with TEM_{00} modes, locking to these will prevail given their larger locking range. Actually, a two-way spatial filtering effect occurs, which enhances an even very approximate mode matching, since the feedback from an excited cavity mode must itself match the laser cavity in order to maximize feedback.

For this application we use DFB lasers packaged without fiber or optical isolator, and we mount them on a small single-stage Peltier inside a home-made housing which includes an aspheric collimating lens. This housing is sufficiently compact to be fixed on a tilt stage, so that it is sufficient to use just another steering mirror to align the laser beam along one of the V-cavity axes. The laser housing is air-tight, allowing a large temperature range for the laser (from -10 to $60\,^{\circ}$C) without water-condensation effects at low temperatures.

The cavity mirrors are glued inside metal holders which permit vacuum-tight mounting on the cavity assembly and also their easy removal for cleaning without losing alignment. Metal tubes (5-mm internal diameter) for the two cavity arms are glued onto a specially machined piece containing a hol-

low V-junction. A small cell volume is thus obtained (about 15 cm^3).

For compactness, electronic cards for laser-temperature control and pulsed current generation are installed inside the chassis of a 486 computer, which is equipped with A/D (12-bit, 1-MHz) and D/A (two 16-bit channels) interface PC cards for data acquisition and system control. As in the cw-CRDS setup, real-time ringdown sampling and fitting are used to obtain spectra of one or two absorption lines and to determine trace concentrations of the corresponding species from line-shape fitting.

4   Examples of applications to trace detection

4.1   *CW-CRDS*

Our cw-CRDS setup has two interesting features for application to high-resolution measurements. The first is a consequence of the fact that most telecom DFB lasers do not present mode hops in their whole operating range. Our tests with DFBs from different companies confirmed continuous tuning over more than 5 nm by scanning the operating temperature from 0 to 60 °C. The second feature is that a fibered setup allows easy replacement of the DFB laser to extend the spectral range. For instance, we are presently scanning the water-vapor spectrum at low pressure, using 31 DFB lasers to go from 1480 to 1630 nm. The goal is to improve the spectral data available in the HITRAN 2000 database (www.hitran.com).

Examples of temperature-tuned spectra for different samples filling the ringdown cavity at room pressure and temperature are shown in Fig. 4. Each scan took about 20 min, with each point obtained by averaging ringdown times from 100 ringdown events. The noise level is 1.4×10^{-9} /cm, from the standard deviation of a linear fit to a flat section of spectrum baseline. Considering the data rate ($\sim$ 6 points/s) the bandwidth-normalized noise level is about 5×10^{-10} cm^{-1} Hz$^{-1/2}$, which compares favorably with typical cw-CRDS results from previous works (taking into ac-
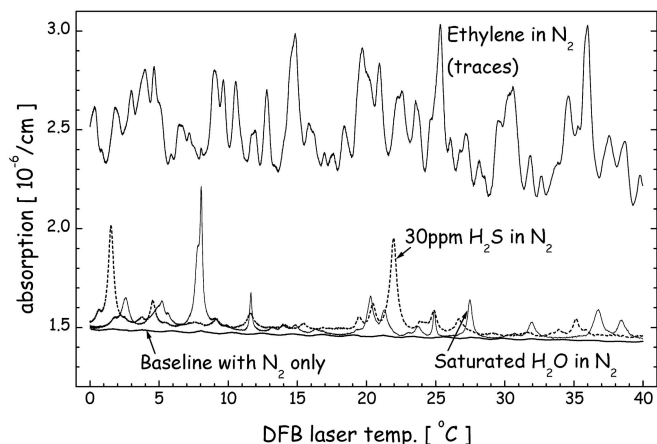

FIGURE 4 Raw spectra from the fibered cw-CRDS setup using laser-temperature scans. The ringdown cell was filled with different gas samples at room pressure and temperature. A scan with dry nitrogen flow was used for the baseline spectrum (also plotted). The ethylene spectrum was obtained after injecting a trace amount of this molecule into the nitrogen flow, which was then interrupted for the duration of the scan

count the 22-μs ringdown time obtained with our mirrors and cavity length). The high sensitivity allows for high-quality spectra even with very low concentrations, e.g. 30 ppm in the case of H_2S. Indeed, ppm-level concentrations are detectable for most species possessing strong first-overtone transitions around 1.6 μm (from stretch vibrations involving a hydrogen atom). The spectra plotted in Fig. 4 are raw data, with no smoothing or baseline correction. The baseline, also plotted, was obtained with a N_2 flow. On this baseline one can notice small oscillations of about 2 °C period: these are due to etaloning inside the mirror substrates, a well-known effect in CRDS [4]. This oscillating baseline is perfectly reproducible even after several cycles of filling-and-flushing the cavity. Independent baseline determination is really necessary when lines are strongly blended, as in the case of ethylene (also shown in the figure).

In order to determine the absorption dynamic range, we injected enough CO_2 to push some absorption lines to the limit when cavity injection at the line peaks becomes very weak. Absorption in excess of 10^{-5} cm could still be measured, as shown in Fig. 5. Considering the baseline noise level given above, the dynamic range thus extends over four orders of magnitude. The true limit to the cw-CRDS dynamic range actually depends on many parameters. For instance, the ringdown time becomes shorter (and the signal intensity lower) as intracavity absorption increases, which demands a faster photodiode amplifier and a faster digitizer. If one wishes to pay for state-of-the-art technology, the dynamic range could perhaps be increased by another order of magnitude.

In Fig. 5 we also plot a spectrum simulated using line widths and strengths from the HITRAN database (with Lorentzian line shapes). Even without wavelength linearization, the temperature dependence of the DFB wavelength is sufficiently linear for a direct comparison by just stretching the wavelength scale. Concentrations of different species in the simulation are adjusted until good agreement is obtained (here, 5200 ppm for CO_2 plus 13.5 mbar for H_2O, which corresponds to about 50% of relative humidity at 22 °C). Indeed, most line intensities and widths are found to agree to better

than 1%. This is true for lines with large intensity differences, which confirms the linear response of CRDS over its whole dynamic range.

Reproducibility may be assessed by comparing successive spectra obtained in the same conditions (flowing nitrogen saturated with water vapor by using a water bubbler and a filter). As shown in Fig. 6, after a delay of about 30 min the difference between spectra is just two or three times above the noise level ($\sim 10^{-9}$ /cm). Comparison with a HITRAN simulation (using 27 mbar of saturated vapor pressure at 22 °C, very close to the temperature in our laboratory) shows that half of the lines are missing from the database, including rather strong ones. Indeed, this is an interesting region for the modeling of atmospheric extinction since it is a water-vapor transparency window. This motivated us, as mentioned above, to exploit this device as a spectrometer (coupled with a Fabry–Perot etalon for precise scan linearization) to refine the HITRAN database in the telecom range. Finally, in Fig. 6 a stick spectrum is also reproduced, which was obtained from Schwenke and Patridge [50]. Its excellent agreement with the CRDS data shows that most of the lines missing in HITRAN are actually expected from high-quality calculations.

With respect to the accuracy of trace measurements, we made tests with calibrated CO_2 samples of 36.7, 350, and 488 ppm in dry air (2% calibrated samples by Messer). The concentration was deduced from a Lorentzian line-shape fit (including a second-order polynomial baseline) to the rather well-isolated CO_2 line at 1579.14 nm, having peak absorption 1.78×10^{-9} cm^{-1} ppm^{-1} at STP according to HITRAN. This value had to be adjusted in order to obtain agreement with the 488-ppm sample. Then, agreement to within sample accuracy was found for the other two samples. As the samples were flushed through the cell at room temperature and pressure, a correction was applied for line-strength dependence on temperature (no correction was needed for pressure variations). Observed day-to-day reproducibility was ±0.3% (peak-to-peak variation of measured CO_2 concentration during 1 month
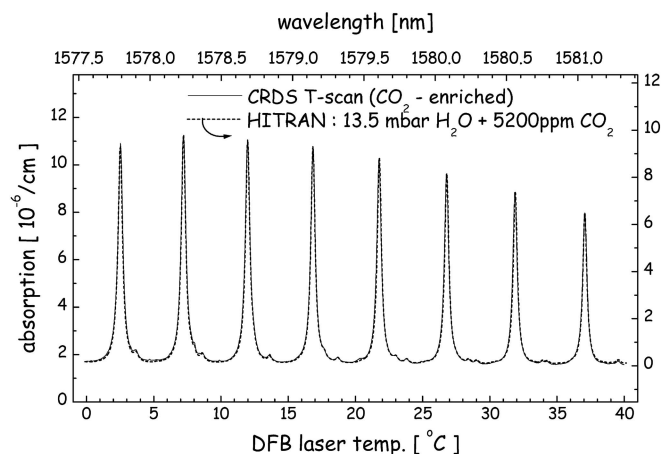

FIGURE 5   Illustration of dynamic range and linear response of cw-CRDS. Spectra (laser-temperature tuning) are from CO_2-enriched air. No baseline correction or smoothing is applied. A simulated HITRAN 2000 spectrum superposes almost perfectly to the data (wavelength scale at *top*) even for lines which get close to the maximum detectable absorption
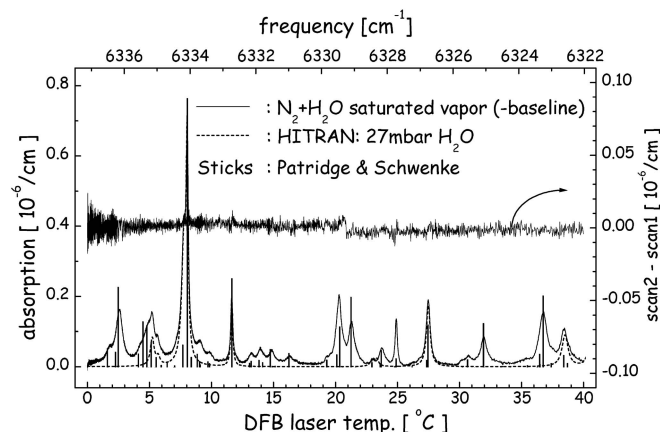

FIGURE 6   CW-CRDS spectrum obtained with a flow of nitrogen saturated by water vapor at room pressure and temperature. A baseline obtained with dry nitrogen flow was smoothed and subtracted. The difference between two successive scans is also shown with enlarged scale (on the *right-hand side*). A HITRAN 2000 simulation (*upper* wavelength scale) shows that almost half of the water lines are missing from the database in this spectral region. The stick spectrum is from [50], and shows that most of these missing lines were predicted by the theory

of testing). At a flow rate of 50 cc/min (used to limit sample consumption), the delay or 'memory time' for a stable reading after sample change was about 2 min. For one measurement, the laser current was tuned in about 1.5 s across the absorption line to give 100 points with 10 ringdown events averaged per point. Faster scans are possible, but in our setup these induce slight oscillations of the laser temperature giving a distorted line shape. We used a Fabry–Perot etalon to sample once and for all the laser frequency tuning curve as a function of injection current. This was fitted to a polynomial function to be used for frequency linearization before each line-shape fit. We observed that the frequency-tuning curve unfortunately presents slight sinusoidal oscillations (about one period over the absorption line width) which cannot be included in the linearization function since they slowly drift in time. These are due to weak optical feedback to the laser from some very close optical element, probably inside the DFB package itself. At this time we do not correct for this effect, but we estimate that it limits the accuracy of the line-shape fit only when the spectra are averaged over more than 10 s.

Finally, we tested the effect of averaging on noise level (signal fluctuations on the spectrum baseline) and also on the standard deviation of the absorption line-shape fit. The relative noise level on the ringdown rate for a single exponential fit is on the order of 0.2%, which reflects the intrinsic noise on the ringdown signal. Shot-to-shot fluctuations are not much larger than this limit, about 0.4%. Averaging was found to decrease the noise according to the statistical rule $1/\sqrt{N}$ up to $N \sim 50$, after which saturation occurred due to the presence of small baseline oscillations of short period (from diffused light at the input to the APD fiber). This is the same effect as the slower oscillations discussed above, but since the distance from the cavity to the fiber fluctuates in time, these oscillations are not reproducible. They constitute the major source of noise in our device at this time, and we plan to replace the fiber whose input surface is spoiled. This should allow coming closer to the 0.2% per-shot limit, but it should even more significantly reduce noise on strongly averaged spectra obtained by temperature scans.

4.2   OF-CRDS

We present here examples of results from three of-CRDS setups based on DFB lasers at 1.31, 1.65, and 1.66 μm. We did not use fibered lasers for this application since the practical advantage of fibered optics is not evident in of-CRDS. The main problem is that fibered telecom diodes usually include an optical isolator which would stop most of the optical feedback from the cavity resonances.

Principal advantages of of-CRDS, apart from the limited number of components and their lower cost, are the high ringdown acquisition rate and the insensitivity to vibrations. Actually these are even needed to produce laser–cavity distance fluctuations. Hence, of-CRDS is well adapted to monitor fast changes in gas concentration and to work in noisy environments.

1.312 μm is a convenient wavelength for HF detection. Since this molecule strongly reacts with cell and mirror surfaces, we use an open-path V-cavity. Two identical devices were realized and deployed for field measurements during one

month, with several hours of operation per day [51]. In order to protect the mirrors from dust, in these devices a flow of filtered air is injected close to the high-reflectivity surfaces of the mirrors (slightly reducing the effective sample absorption path). No mirror cleaning was needed during the whole measurement campaign, while optical alignment was optimized only two or three times. An interesting issue with open-path ringdown is the presence of spikes on the spectra, caused by the passage of dust particles inside the open cavity. These spikes have a duration of several ms, thus affecting several points on a 200-ms scan. These spikes are easily removed by comparing two or three scans and taking the minimum value for each spectral point, rather than performing a simple average. A reduced data rate is thus the price to pay.

For the measurements in Fig. 7 an open stainless steel tube was temporarily placed along one arm of the V-cavity. After injecting a small amount of HF into this tube, spectra (around 1312.2 nm) were recorded and fitted with a response time of 1 s. In Fig. 7a we present the evolution of the concentration after HF injection. In Fig. 7b is shown a sample of the HF spectra obtained for different HF concentrations. As a water line is present close to the HF line, this is taken into account in the fitting procedure, providing a simultaneous de-
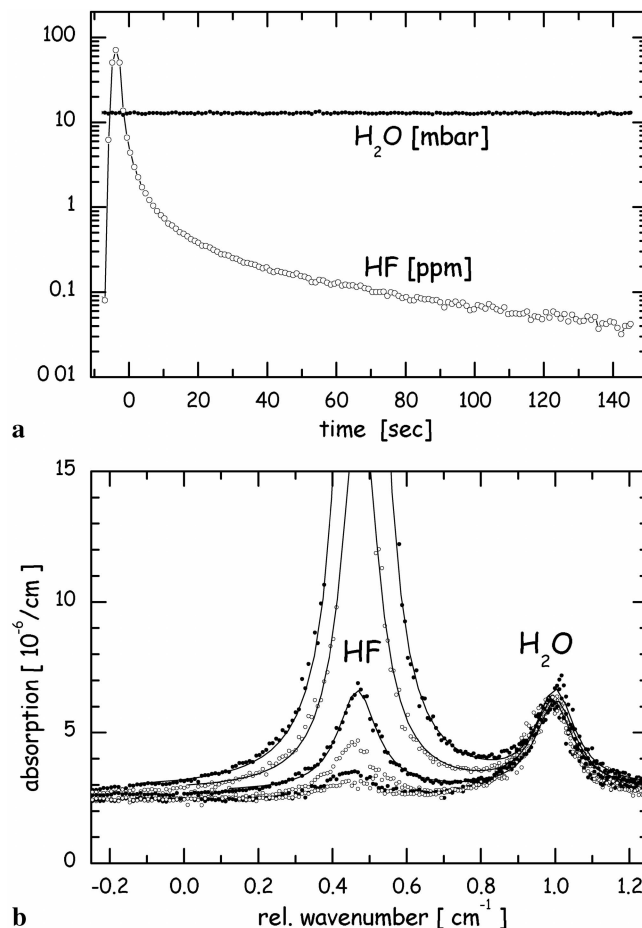

FIGURE 7 **a** Evolution of HF and H_2O concentrations measured after HF injection in the open-path V-cavity (1 s per data point). **b** HF spectra recorded at successive times after HF injection. For high concentrations only the wings of absorption lines are available for line-profile fitting (fitted curves are plotted in *continous lines*)

termination of the water-vapor concentration (also plotted in Fig. 7a).

As noted previously, when an absorption line becomes too strong, its complete profile cannot be recovered since the feedback level, and hence the locking range, becomes too weak at the line center. The concentration of the absorber is however determined from a Lorentzian fit, which keeps working on the wings of the collisional profile. This significantly increases the dynamic range of concentration measurements, which extends for HF from 50 ppb to 80 ppm (where noise on the concentration data starts increasing). At the same time we observe a good reproducibility in the simultaneous water measurement (about 1% noise level). It should be remarked that, as averaging reduces the noise level, it also increases the dynamic range. Response time and dynamic range are thus partially dependent.

In Fig. 8, we present ambient-air spectra from a closed V-cavity of-CRDS device, showing the isolated R_4 methane multiplet at 1650.5 nm (which belongs to the $2\nu_3$ transition). The scan range of approximately $1.3\,\mathrm{cm}^{-1}$ corresponds to a laser-current excursion of 50 mA. The feedback rate is adjusted for a pulse duration of $\sim 250\,\mu s$. The laser-off duration ($\sim 100\,\mu s$) is limited by the need to sample a sufficient portion of the ringdown decay for fitting. As explained before, sufficiently strong ringdown signals are sampled for 70 to 80% of the pulses. Keeping into account delays due to numerical treatment of the data, the effective acquisition rate of the ringdown events is about 1 kHz. Together with the noise level evaluated on the spectrum baseline (2.5×10^{-8} /cm), this gives a normalized detection limit of less than $10^{-9}\,\mathrm{cm}^{-1}\,\mathrm{Hz}^{-1/2}$. For a ringdown time of only 14 μs this is a very respectable performance.

The standard deviation of the ringdown rate from the fit of a single ringdown is <0.1%, but the noise measured on the spectrum baseline, reflecting shot-to-shot variations, is about 2%. As discussed, this is due to a loss difference for odd/even cavity modes. Given the random nature of odd/even mode sampling, averaging is effective in decreasing this noise, as illustrated by the 256-times averaged spectrum in Fig. 8.
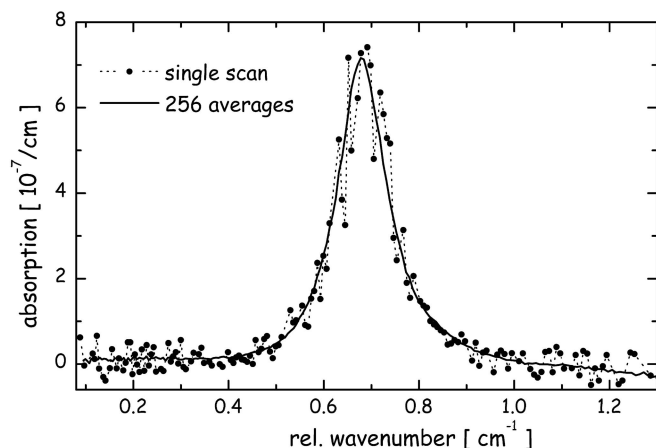
A characterization of the noise as a function of averaging shows that this follows the $1/\sqrt{N}$ law, where N is the number of ringdowns averaged per data point, up to practical values of $N \sim 1000$. A noise-equivalent absorption of 5×10^{-10} /cm has been observed by 5-min averaging of this spectrum.

Measurements of ambient methane for two integration times (Fig. 9) show that the $1/\sqrt{N}$ noise dependence seems to hold also for the concentration determined from line fitting. However this stops for averaging times above 10 s, where the residuals to the line fit start displaying systematic line-shape distortions. These are due to imperfection in the laser-current tuning and to baseline etaloning effects, such as described in the cw-CRDS case.

In order to check the linear response of of-CRDS, we used samples of 600, 160, 50, 20, and 3 ppm of methane obtained by successive dilutions. Fig. 10 displays the excellent agreement between each raw spectrum and the one obtained by scaling a lower-concentration spectrum by the ratio of the respective concentrations. For example, the 50-ppm spectrum scaled by 160/50 superposes closely with the 160-ppm spectrum.

Finally, we present in Fig. 11 a water-vapor spectrum obtained with a closed V-cavity system working around
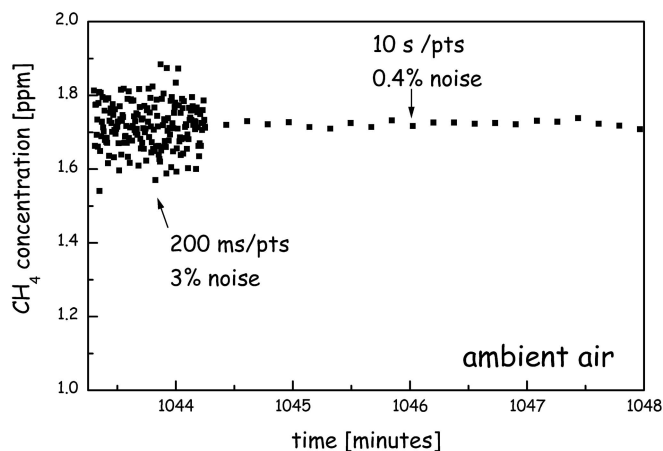

FIGURE 9   Measurement of methane concentration in ambient air for two response times and averaging. Noise drops according to the $1/\sqrt{N}$ law
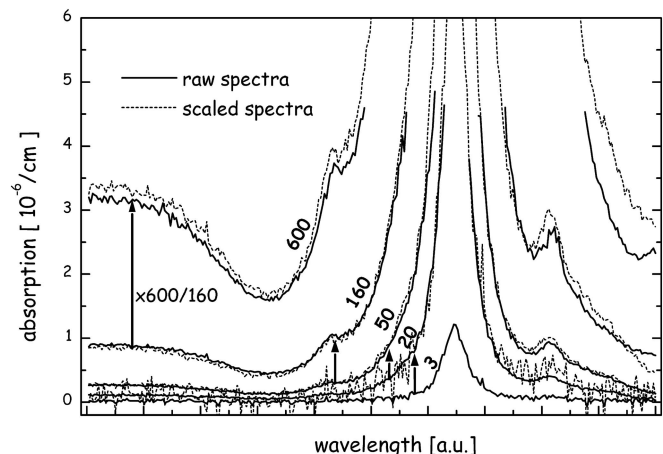

FIGURE 8   OF-CRDS spectra of CH$_4$ around 1650.5 nm. In *black dots* is a single scan acquired in 200 ms. The *solid-line* spectrum is averaged over 50 s. Baseline noise on a single scan is about 2.5×10^{-8} /cm, and drops to 1.9×10^{-9} /cm in the averaged spectrum, consistently with random noise averaging

FIGURE 10   Test of the of-CRDS linear response using calibrated methane samples with 600, 160, 50, 20, and 3 ppm. Absorption line is the R_4 at 1650.5 nm. See text for details
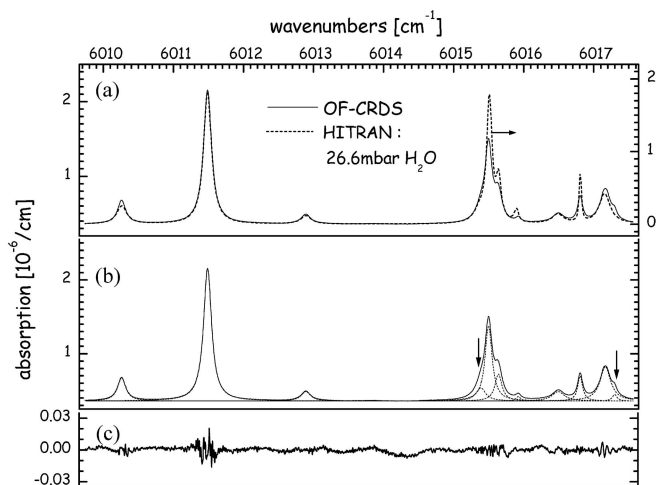
FIGURE 11 (a) Comparison of of-CRDS saturated water spectra against simulations from the HITRAN 2000 database. The frequency scale was linearized by using a Fabry–Perot etalon. (b) Fit with 11 Lorentzian line profiles, whose residuals are given in (c)

1662 nm. In order to obtain a larger spectral range for comparing with a HITRAN simulated spectrum, the laser was tuned by temperature (from about 13 to 35 °C) while the amplitude of current pulses was kept constant. Temperature tuning had to be done rather slowly, small steps were used (0.0075 °C), and 50 ringdown events where averaged per data point. A scan took about 7 min. A beam splitter was installed to direct a fraction of the laser beam to a solid Fabry–Perot etalon (3-cm thick) and a photodiode, producing fringes for linearizing the scan-frequency scale. A flow of nitrogen saturated by water vapor at room temperature and pressure was injected into the device (same procedure as used for Fig. 6). A baseline was obtained by flowing dry nitrogen, and subtracted from the water spectra to eliminate small baseline oscillations. It is to be noticed that successive scans after the water-saturated flow was started were very reproducible except for a baseline offset slowly but steadily increasing with time. We attribute this to condensation effects over mirror surfaces and possibly in the cell volume. Flushing with dry nitrogen would systematically re-establish the original baseline level.

The measured temperature of the water bath was 21 °C, giving a saturated water pressure of 25.1 mbar. However the best agreement with the strongest line (at 6011.5 cm^{-1}) could be obtained for a HITRAN simulation (also plotted in panel (a) of Fig. 11) with a water pressure of 26.6 mbar. In addition the overall agreement is less good than for the comparison in Fig. 6, both with respect to line intensity and positions. We attribute this mismatch to the lower quality of HITRAN data in this spectral region given the reproducibility of water spectra by our device and by its highly linear response. In panel (b) of Fig. 11, we present the result of fitting the entire spectrum by Lorentzian profiles and in (c) the fit residues. Eleven lines are necessary to fully describe the spectrum. In particular, two weak lines (marked by arrows) partially blended with stronger ones, must be included. These are not reported by the database but are predicted by the ab-initio calculations of Schwenke and Patridge [50].

5   Conclusions and perspectives

We presented two injection schemes of a high-finesse cavity for ringdown measurements with DFB diode lasers. We reported several results from different compact setups, which demonstrate high performance in terms of sensitivity and time response. Specific problems, whose solution will increase performance of both systems, were outlined. We recall here the main features which make each of these schemes more or less adapted to different applications, and also discuss some future possibilities.

The high spectral resolution of cw-CRDS makes it appropriate for high-accuracy trace-gas measurements especially at low pressure. On the other hand, we have seen that a large frequency noise does not make spectral resolution a strong point in favor of of-CRDS. Working at low pressure is actually a valuable trick for improving separation of absorption lines and thus the accuracy of concentration measurements [22]. It is to be noted that, as long as collisional dominates over Doppler broadening, the peak value of isolated absorption lines decreases just slightly with decreasing pressure (at constant relative concentration). Thus, lower pressure does not necessarily imply a loss in detection limit.

With regard to sensitivity, the of-CRDS signal has intrinsically larger pulse-to-pulse fluctuations, which are partly reduced by fast data acquisition and averaging. This gives a normalized detection limit not far from what we have for cw-CRDS when applied to DFB laser diodes. We currently achieve close to 10^{-10} cm^{-1} Hz$^{-1/2}$ for cw-CRDS only when using higher-power (> 20 mW) telecom diode lasers in our fibered setup. This shows that the main problem is the low signal level when no optical feedback is used to enhance cavity injection. Actually, a cw-CRDS industrial prototype was recently described [22], having a detection limit still about 10 times better than this. However, that system includes an ECDL, which allows better cavity injection at the passage through resonance. In addition, improved performance is to be attributed to professional engineering and optimization of electronics and data processing.

For cw-CRDS a fibered setup was proposed to allow setting up a compact and robust system. An interesting extension is using more than one DFB laser to detect different molecules with the same device, choosing wavelengths inside the working range of the cavity mirrors [1]. Emission from these lasers could be injected into the same fiber by a fiber commutator or by a fiber mixer, and their operation could be multiplexed in time to benefit from the same AOS, photodiode, and signal-processing chain.

With of-CRDS, a compact and robust setup was obtained without need for fibered components, which also contributes to reducing costs. Indeed, of-CRDS needs very few optical components: a DFB laser, a steering mirror, an attenuator, a V-shaped ringdown cavity, and a photodiode. Even without fibers it is possible to conceive a multi-wavelength version of the of-CRDS device. For example, a multi-beam Fresnel splitter could be used to mix several lasers, since a small fraction of the signal from each is actually needed for cavity injection by optical feedback. Time multiplexing would then allow separating the operation of these sources.

Flowing the sample through the ringdown cavity was used in both schemes. A mechanical filter with micron-size pores was sufficient for eliminating dust particles which in the long run soil mirror surfaces but also produce sudden jumps in the ringdown time, giving spikes in the absorption spectra. It is indeed interesting that CRDS can be used as a sensitive probe for aerosol particles, but it is not clear how to extract quantitative information about e.g. particle-size distribution. In practice, tests done with ambient air and a 3-μm-pore filter showed that a continuous flow of a few liters/min for more than one month goes without appreciable degradation of the ringdown time. An open-path ringdown cell could also be used in dust-free environments (clean rooms, stratosphere, etc.), or when the gas to detect is very sensitive to surfaces (strongly polar or reactive molecules such as H_2O, HF, etc.). In this case, we have shown that a clean gas flow on the mirror surfaces is an effective protection. This solution would be impractical in a multi-pass cell, given the much larger mirror size. We have also shown how spikes produced by dust particles may be removed at the data-processing stage, with some sacrifice of data-acquisition rate.

All considered, of-CRDS wins in terms of setup simplicity, robustness, and cost. However, in the present configuration it does not seem that it can compete with cw-CRDS in terms of sensitivity, especially if an ECDL is employed in place of a DFB laser [22]. With respect to application of of-CRDS to other types of lasers, the main requirement is the sensitivity to optical feedback. Quite obviously, of-CRDS should work with DFB diode lasers based on technologies different from InGaAs (telecom devices). Indeed, we recently successfully tested of-CRDS with a GaSb quantum-well DFB diode laser working at 2.35 μm [52]. We should also consider simple Fabry–Perot (FP) diode lasers, external cavity diode lasers (ECDLs), and quantum cascade lasers (QCLs).

An important characteristic of DFB lasers as compared to FP diode lasers is their higher stability in presence of optical feedback. For good performance of of-CRDS, optical feedback on the level of 10^{-3} is needed. This feedback occurs only at cavity resonances, and the large side-mode suppression in DFB lasers (60 dB typically) allows single-mode operation with resonant feedback rates exceeding 10^{-2}. This could induce mode hops and even chaotic behavior in a FP diode, whose side-mode suppression is not very good. We believe however that of-CRDS with FP diodes is possible, but using low feedback rates which would imply a small locking range and a relatively low repetition rate.

The sensitivity of ECDLs to optical feedback is lower than for DFBs. We have performed successful preliminary tests with an ECDL at 670 nm. It appears that in order to obtain a locking range close to the cavity FSR one needs to use almost no attenuation for the feedback.

With respect to QCL technology, hopes are high that mid-infrared trace detection could benefit from of-CRDS coupled with such sources. One of the main advantages is the large cavity injection which would compensate for the low quantum efficiency of detectors in that spectral range.

A last word about cw-CRDS. This scheme has the advantage of working with any single-frequency laser, which makes it an indispensable laboratory technique for high-sensitivity,

high-resolution absorption spectroscopy especially when the sample is a supersonic jet or is available in limited amounts (isotopically substituted species). In addition, when high spectral resolution is not needed (spectroscopy of broad absorption spectra), this scheme will also work with cw lasers which are not single-frequency, e.g. most entry-level versions of commercial cw dye lasers. Such lasers operate on several longitudinal modes and cavity injection will be observed when one of these modes passes through resonance with a cavity mode. Cavity-length modulation should still be useful to obtain frequent passages through resonance, and interruption of the laser beam would still produce a ringdown at a wavelength somewhere inside the laser-emission spectrum. To our knowledge such a scheme has not been exploited until now, but it should not present particular difficulties, except for transverse mode matching which might become impossible to achieve. In fact, the cavity transmission pattern used to monitor the transverse-mode excitation with a single-frequency laser would become almost unreadable.

REFERENCES

1 G. Totschnig, D. Baer, J.W.A.F. Winter, H.H.R.K. Hanson: Appl. Opt. **39**, 2009 (2000)
2 A. O'Keefe, D.A.G. Deacon: Rev. Sci. Instrum. **59**, 2544 (1988)
3 A. O'Keefe, J.J. Scherer, A.L. Cooksy, R. Sheeks, J. Heath, R.J. Saykally: Chem. Phys. Lett. **172**, 214 (1990)
4 D. Romanini, K.K. Lehmann: J. Chem. Phys. **99**, 6287 (1993)
5 T. Yu, M.C. Lin: J. Am. Chem. Soc. **115**, 4371 (1993)
6 G. Meijer, M.G.H. Boogaarts, R.T. Jongma, D.H. Parker, A.M. Wodtke: Chem. Phys. Lett. **217**, 112 (1994)
7 D. Romanini, K.K. Lehmann: J. Chem. Phys. **102**, 633 (1995)
8 J.T. Hodges, J.P. Looney, R.D. van Zee: *Ohio State University International Symposium on Molecular Spectroscopy* (T.A. Miller, Department of Chemistry, Ohio State University, Columbus, OH 1998)
9 P. Zalicki, R.N. Zare: J. Chem. Phys. **102**, 2708 (1995)
10 J.J. Scherer, D. Voelkel, D.J. Rakestraw, J.B. Paul, C.P. Collier, R.J. Saykally, A. O'Keefe: Chem. Phys. Lett. **245**, 273 (1995)
11 J. Pearson, A.J. Orr-Ewing, M.N.R. Ashfold, R.N. Dixon: J. Chem. Soc. Faraday Trans. **92**, 1283 (1996)
12 M. Kotterer, J. Conceicao, J.P. Maier: Chem. Phys. Lett. **259**, 233 (1996)
13 R. Engeln, G. Meijer: Rev. Sci. Instrum. **67**, 2708 (1996)
14 D. Romanini, A.A. Kachanov, N. Sadeghi, F. Stoeckel: Chem. Phys. Lett. **264**, 316 (1997)
15 D. Romanini, A.A. Kachanov, F. Stoeckel: Chem. Phys. Lett. **270**, 538 (1997)
16 D. Romanini, A.A. Kachanov, F. Stoeckel: Chem. Phys. Lett. **270**, 546 (1997)
17 A.C.R. Pipino, J.W. Hudgens, R.E. Huie: Rev. Sci. Instrum. **68**, 2978 (1997)
18 R.D. van Zee, J.T. Hodges, J.P. Looney: Appl. Opt. **38**, 3951 (1999)
19 D. Romanini, L. Biennier, F. Salama, A. Kachanov, L.J. Allamandola, F. Stoeckel: Chem. Phys. Lett. **303**, 165 (1999)
20 J.J. Scherer, J.B. Paul, H. Jiao, A. O'Keefe: Appl. Opt. **40**, 6725 (2001)
21 S.M. Ball, I.M. Povery, E.G. Norton, R.L. Jones: Chem. Phys. Lett. **342**, 113 (2001)
22 E.R. Crosson, K.N. Ricci, B.A. Richman, F.C. Chilese, T.G. Owano, R.A. Provencal, M.W. Todd, J. Glasser, A.A. Kachanov, B.A. Paldus, T.G. Spence, R.N. Zare: Anal. Chem. **74**, 2003 (2002)
23 D. Romanini: in *Cavity-Ringdown Spectroscopy – A New Technique for Trace Absorption Measurements*, ed. by K.W. Busch, M.A. Busch (American Chemical Society, Washington, DC 1998)

24 A. Campargue, D. Romanini, N. Sadeghi: J. Phys. D: Appl. Phys. **31**, 1168 (1998)

25 R.E. Engeln, G. von Helden, G. Berden, G. Meijer: Chem. Phys. Lett. **262**, 105 (1996)

26 B.A. Paldus, C.C. Harb, T.G. Spence, B. Wilke, J. Xie, J.S. Harris, R.N. Zare: J. Appl. Phys. **83**, 3991 (1998)

27 Y. He, B.J. Orr: Chem. Phys. Lett. **319**, 131 (2000)

28 Y. He, B.J. Orr: Chem. Phys. Lett. **335**, 215 (2001)

29 Y. He, M. Hippler, M. Quack: Chem. Phys. Lett. **289**, 527 (1998)

30 D. Romanini, P. Dupré, R. Jost: Vib. Spectrosc. **19**, 93 (1999)

31 M. Hippler, M. Quack: Chem. Phys. Lett. **314**, 273 (1999)

32 H. Dahnke, D. Kleine, P. Hering, M. Mürtz: Appl. Phys. B **72**, 971 (2001)

33 T.G. Spence, C.C. Harb, B.A. Paldus, R.N. Zare: Rev. Sci. Instrum. **71**, 347 (2000)

34 L. Biennier, D. Romanini, A. Kachanov, A. Campargue, B. Bussery-Honvault, R. Bacis: J. Chem. Phys. **112**, 6309 (2000)

35 D. Romanini, A. Kachanov: French Patent 9805753, Laboratoire de Spectrométrie Physique – UJF Grenoble (unpublished)

36 D. Romanini, A.A. Kachanov, J. Morville, M. Chenevier: Proc. SPIE **3 821**, 94 (1999) [Proc. SPIE EUROPTO Ser., Environmental Sensing and Applications]

37 J. Morville, M. Chenevier, A.A. Kachanov, D. Romanini: SPIE Proc. Ser. **4485**, 236 (2001)

38 K. Busch, M. Busch: in *Cavity-Ringdown Spetroscopy – An Ultratrace-Absorption Measurement Technique*, ed. by K. Busch, M. Busch (American Chemical Society, Washington, DC 1999)

39 G. Berden, R. Peeters, G. Meijer: Int. Rev. Phys. Chem. **19**, 565 (2000)

40 P. Dupré: C. R. Acad. Sci. **2**, 929 (2001)

41 D.Z. Anderson, J.C. Frisch, C.S. Masser: Appl. Opt. **23**, 1238 (1984)

42 B.L. Fawcett, A.M. Parkes, D.E. Shallcross, A.J. Orr-Ewing: Phys. Chem. Chem. Phys. **4**, 5960 (2002)

43 J. Morville, D. Romanini, M. Chenevier, A. Kachanov: Appl. Opt. **41**, 6980 (2002)

44 C.E. Wieman, L. Hollberg: Rev. Sci. Instrum. **62**, 1 (1991)

45 C. Tanner, B. Masterson, C. Wieman: Opt. Lett. **13**, 357 (1988)

46 P. Laurent, A. Clairon, C. Breant: IEEE J. Quantum Electron. **QE**-25, 1131 (1989)

47 H. Li, N. Abraham: IEEE J. Quantum Electron. **QE**-25, 1782 (1989)

48 H. Li, H. Telle: IEEE J. Quantum Electron. **QE**-25, 257 (1989)

49 J. Morville: Ph.D. thesis, Universite Joseph Fourier, Grenoble, France, 2001

50 D.W. Schwenke, H. Patridge: J. Chem. Phys. **113**, 6592 (2000)

51 D. Romanini, J. Morville, M. Chenevier: submitted to J. Hazard. Mater. (2003)

52 Y. Rouillard, F. Genty, A. Perona, A. Vicet, D.A. Yarekha, G. Boissier, P. Grech, A.N. Baranov, C. Alibert: Philos. Trans. Math. Phys. Eng. Sci. **359**, 581 (2001)